THE JOURNAL OF PHYSICAL CHEMISTRY C

Subscriber access provided by UNIV COLL CORK

C: Surfaces, Interfaces, Porous Materials, and Catalysis

Coverage and Stability of NH Terminated Cobalt and Ruthenium Surfaces: A First Principles Investigation

Ji Liu, and Michael Nolan

J. Phys. Chem. C, **Just Accepted Manuscript** • DOI: 10.1021/acs.jpcc.9b06287 • Publication Date (Web): 24 Sep 2019

is published by the American Chemical Society. 1155 Sixteenth Street N.W., Washington, DC 20036

Coverage and Stability of NH_x Terminated Cobalt and Ruthenium Surfaces: A First Principles Investigation

Ji Liu[a] and Michael Nolan[a,*]

[a] Tyndall National Institute, University College Cork, Lee Maltings, Dyke Parade, Cork, T12 R5CP, Ireland

Corresponding author:

[*]E-mail: Michael.nolan@tyndall.ie. Tel: +353 021 2346983

Abstract

In the atomic layer deposition (ALD) of Cobalt (Co) and Ruthenium (Ru) metal using nitrogen plasma, the structure and composition of the post N-plasma NH_x terminated (x = 1 or 2) metal surfaces are not well known but are important in the subsequent metal-containing pulse. In this paper, we use the low-index (001) and (100) surfaces of Co and Ru as models of the metal polycrystalline thin films. The (001) surface with a hexagonal surface structure is the most stable surface and the (100) surface with a zigzag structure is the least stable surface but has high reactivity. We investigate the stability of NH and NH_2 terminations on these surfaces to determine the saturation coverage of NH_x on Co and Ru. NH is most stable in the hollow hcp site on (001) surface and the bridge site on the (100) surface, while NH_2 prefers the bridge site on both (001) and (100) surfaces. The differential energy is calculated to find the saturation coverage of NH and NH_2. We also present results on mixed NH/NH_2-terminations. The results are analyzed by thermodynamics using Gibbs free energies (ΔG) to reveal temperature effects on the stability of NH and NH_2 terminations. Ultra-high vacuum (UHV) and standard ALD operating conditions are considered. Under typical ALD operating conditions we find that the most stable NH_x terminated metal surfaces are 1ML NH on Ru(001) surface (350K-550K), 5/9ML (0.56ML) NH on Co(001) surface (500K-650K) and a mixture of NH and NH_2 on both Ru(100) and Co(100) surfaces.

1. *Introduction*

With the downsizing of semiconductor devices, the copper interconnect becomes the key challenge and the volume available in the via is reduced.[1-3] Barrier and liner layers are needed to prevent copper diffusion and to promote copper adhesion or wetting. Future developments in this area envisage replacing copper with metals such as Co or Ru which have lower resistivity at typical device dimensions. Co can be used as a seed layer for metallization of interconnects and Ru is a potential electrode material for DRAM capacitors and MOSFETs.[4] In modern device structures, the barrier and liner layers and the interconnect require high conformality and continuous thin film deposition at the atomic scale. Atomic layer deposition (ALD) is the leading technique for depositing thin films with these properties in semiconductor technology.[5-6] ALD usually consists of two half-cycle reactions that are each self-limiting with a purge after each step. The reactions stop when all available surface sites are consumed and this self-limiting property can ensure, at least in principle, that the thickness of the deposited thin film is precisely controlled by changing the number of cycles.[7-8] ALD is used in depositing metal oxides[9-11] (e.g. TiO_2), metal nitride[12] (e.g. TaN), and metals[13-14] (e.g. Cu).

Plasma enhanced ALD (PE-ALD) is a variant of ALD that allows low-temperature deposition, which can make the ALD process consistent with the permitted processing temperatures in semiconductor device fabrication.[15-16] The plasma source can be oxygen or nitrogen. The O-plasma mechanism has been well-established in recent years.[17-21] The oxygen reactant can be H_2O, O_3, or H_2O_2 to promote metal oxide ALD growth.[1, 22] Hydroxylated (OH-terminated) surfaces are produced after this pulse[21, 23] and hydroxylated metal oxide surfaces have been widely studied both for the ALD process[7, 9-10] and in catalysis for reactions including water-gas shift and photocatalysis[24-26].

However, by contrast, the N-plasma mechanism is not well understood. In particular, the nature and stability of NH_x terminated metal surfaces that would be produced during the N-plasma deposition and required for modelling the N-plasma ALD process are entirely lacking. When depositing metals, such as Co and Ru, the use of N-plasma is preferred because this avoids oxygen contamination and subsequent oxidation of the metal surface. Previous studies have used ammonia adsorption or decomposition on platinum group metal surfaces including Pt, Pd and Rh[27-28] or hexagonal close-packed (hcp) metal surfaces such as Ru[29-30] in catalysis-focused studies. The nature of the most stable NH_x fragment on these metals varies with different surface orientations and the decomposition is structure sensitive.

The ALD of Co uses metal precursors such as cyclopentadienyl dicarbonyl cobalt ($CoCp(CO)_2$) and bis-cyclopentadienyl cobalt ($CoCp_2$)[31-33] and the other precursors are NH_3 or a mixture of N_2 and H_2. The first ALD of Ru used $RuCp_2$ and O_2 as precursors. The reported main byproducts are CO_2 and H_2O. A combination of high O_2 dose and low Ru precursor dose can result in RuO_2 rather than Ru.[4] Other Ru precursors such as $Ru(EtCp)_2$ and $CpRu(CO)_2Et$ have also been developed.[19, 34] Generally, the deposition temperature is above 200°C for these metal precursors.[35-36] As pointed out earlier, oxygen can oxidize metal surface and use of N-plasma is therefore important for the deposition of metals. Experimental results have pointed out that both NH_3-plasma and N_2/H_2 plasma can result in high purity and low resistivity Co thin film. However, H-plasma alone or separate N_2 and H_2 plasma can produce lower purity and higher resistivity Co thin films.[32-33, 37] It has been argued that the NH_x-terminated metal surfaces play an important role in Co thin film deposition.[32, 38] However, the nature of the NH_x-terminated metal surfaces is not yet understood and this is the key advance in our present work.

Density functional theory (DFT) calculations have been successfully applied to reveal the reaction mechanism of O-plasma in PE-ALD.[39-41] However, limited theoretical studies are available that discuss N-plasma PE-ALD.[42] Phung *et al.*[43-44] have simulated the ALD of Ru on

Ru surfaces focusing on Ru precursor reactions with bare Ru surface and H-terminated Ru surfaces. The effect of nitrogen plasma is not considered in that paper. A full ALD cycle is as follows - starting from the post N-plasma cycle, the metal surface will be NH_x-terminated surface, where *x* can be 1 or 2. Then the metal precursors ($RuCp_2$ and $CoCp_2$) are adsorbed on the NH_x-terminated metal surfaces and a hydrogen transfer step can produce CpH which desorbs. The second half reaction with N-plasma produces a deposited metal layer with an NH_x-terminated surface. A whole cycle is completed and the surface is ready for the next cycle. The present paper is focused on using first principles simulations to identify stable NH_x-terminated Co and Ru surfaces by considering termination of Co and Ru with amine (NH_2) or imine (NH) species and mixed termination with NH_2 and NH. The nature and stability of NH_x-terminated metal surface can strongly influence the hydrogen transfer step. The results are further analyzed with ab initio thermodynamics using the Gibbs energy (ΔG) in which the effect of temperature and pressure is considered. The results show that under ALD operating condition, the nature of the NH_x terminated Co and Ru surfaces can be strongly dependent on the temperature at a given pressure. With increasing operating temperature, the surface adsorbed NH or NH_2 may desorb from metal surface. On (001) surface, NH-termination is the most dominant species; while on (100) surface, a mixture of NH and NH_2 is the most dominant species. The study on NH_x terminated metal surface is vital and essential to investigate the PE-ALD deposition of metal thin films.

2. *Methods and Computational Details*

All the calculations are performed on the basis of spin-polarized DFT with the projector augmented wave (PAW) formalism[45], as implemented in the Vienna *ab* initio simulations package (VASP 5.3) code. The generalized gradient approximation (GGA) with the

parameterization of Perdrew-Burke-Ernzerhof (PBE) is used for the exchange-correlation functional.[46-47] The energy cutoff is set to be 400eV for the plane wave expansion. The convergence of energy and forces are set to be 1×10^{-4} eV and 0.01eV/Å, respectively. The bulk Co and Ru crystal structure is optimized by simultaneously relaxing the ionic positions, cell volume and cell shape at a higher plane wave energy cutoff of 550eV and a Monkhorst-Pack grid[48] k-point mesh of 12 × 12 × 6. The resulting lattice constants are a = b = 2.489Å, and c = 4.035Å for Co bulk and a = b = 2.715Å, and c = 4.285Å for Ru bulk.

The deposited Co or Ru films by ALD are polycrystalline and have random surface orientations after low temperature deposition. The Ru crystallite tends to orient towards [001] direction at elevated temperature or increased plasma power.[4] In this paper, three X-ray detected low-index surfaces (001), (100), and (101) are considered. The surface models consist of multi-layer Ru or Co and the vacuum region is up to 15Å. Both (3 × 3) and (4 × 4) surface supercell expansions are considered to minimize the neighboring effect of adsorbates (NH and NH_2). A five-layer slab is used in the (100) and (001) surfaces, and an eight-layer slab is used for the (101) surface. The computational details of these slab model and calculated properties are shown in Table S1 in supporting information. The configurations of these surfaces are shown in Figure 1. The bottom three layers are fixed during the calculations. We have checked the effect of fixing the number of layers on the adsorption energies. The results are summarized in Table S2 in supporting information and show that our model of fixing the bottom three-layers is reasonable and reliable.

Both Ru and Co have the lowest surface energy along [001] direction, which forms a hexagonal structure and is the most stable surface. The (100) surface has a zigzag structure and shows high reactivity, while the (101) surface is a nearly flat surface. Based on the surface stability and reactivity, we have chosen the most stable (001) surface and the least stable, and high reactivity surface, (100) to study the stability of NH_x-terminations.

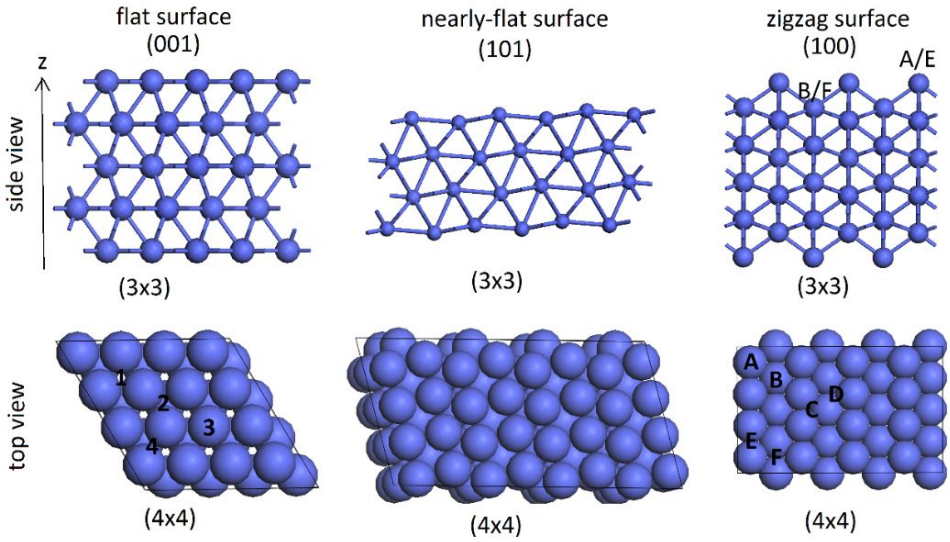

Figure 1. The top and side view of Ru or Co surfaces in three orientations: (001), (101), and (100). The adsorption sites on (001) surfaces are highlighted as 1 (fcc), 2 (hcp), 3 (top), and 4 (bridge); The adsorption sites on (100) surfaces are highlighted as A, B (top), C, D (hollow), and E, F (bridge).

The chemisorption energy of NH_x terminations is defined by the formula:

$$E_{ad} = E_{tot} - E_{slab} - E_A \qquad (1)$$

where E_{tot}, E_{slab}, and E_A are the energy of the metal slab with termination A (A = NH, NH_2), an isolated slab model for the clean metal surface, and isolated adsorbate A, respectively. The reference energy for the NH and NH_2 adsorbate is computed using the total energy of gas phase N_2 and H_2.

$$E_{NH} = \frac{1}{2}(E_{N2} + E_{H2}) \qquad (2)$$

$$E_{NH2} = 1/2E_{N2} + E_{H2} \qquad (3)$$

These correspond to typical gases in the nitrogen plasma set-up. These computed energies can be thought of as an indication of how an NH_x termination resists desorption with temperature, which would be probed through a temperature programmed desorption experiment. At high coverage, the surface NH_x may dissociate into, e.g. NH and H, or form ammonia. The activation

barriers reported in this paper are computed using climbing image nudged elastic band (CI-NEB) method[42] with 6 images including the starting and ending geometries and with force converged to 0.01eV/Å.

3. *Results and Discussions*

3.1 Structure and Stability of NH or NH_2 species at Co and Ru Surfaces

To begin with, we have considered the termination of Co and Ru (001) and (100) surfaces with single NH or NH_2 to assess the preferred binding sites. The possible adsorption sites are shown in Figure 1. For the (001) surfaces, four adsorption sites including hcp, fcc, bridge, and top are considered. On the (100) surface six possible sites are considered, which are top (A and B), hollow (C and D), and bridge (E and F). Due to the unique trench structure of the (100) surface, sites A and E are located on the surface, while site B and F are anchored to zigzag channel. Site E is a surface bridge and site F is a channel bridge. The calculated energies of NH and NH_2 adsorption, relative to $\frac{1}{2}(N_2+H_2)$ and $\frac{1}{2}N_2+H_2$, respectively, are listed in Table 1; to facilitate the discussion, we also align the adsorption energy of the most stable site to be zero as a reference to discuss the stability of NH_x terminations.

The configurations of the most stable single NH and NH_2 terminations on Ru and Co surfaces are shown in Figure 2 and Figure 3, respectively. We see that the most stable binding sites are the same on each surface facet. On the (001) surface, NH prefers to bind on the hcp site while NH_2 prefers to bind on a bridge site. On the (100) surface, both NH and NH_2 prefer a bridge site and these are the bridge F (zigzag channel) for NH and bridge E (surface) for NH_2. A larger surface supercell expansion ((4 × 4) supercell) does not affect the most stable sites and these results are consistent with a previous modelling report on NH_3 synthesis.[29, 49] After relaxation, NH is in an upright position with the nitrogen atom adsorbed on a hollow site on the (001) surface and a channel bridge site on (100) surfaces. The metal-N distances are 1.86Å and 1.89Å

Table 1. The calculated adsorption energies of NH and NH_2 on Co and Ru (001) and (100) surfaces. The energies in bracket are with respect to the energy of most stable site.

	Adsorption energy/eV						
	Co(001)	Co(001)	Ru(001)	Ru(001)		Co(100)	Ru(100)
NH	3×3	4×4	3×3	4×4	NH	3×3	3×3
hcp	-3.68 (0.00)	-3.61 (0.00)	-3.74 (0.00)	-3.68 (0.00)	top_A	-2.29 (1.41)	2.02 (1.56)
bridge	-2.75 (0.93)	-3.14 (0.48)	hollow*	hollow*	top_B	-2.12 (1.58)	-2.49 (1.09)
top	-1.27 (2.41)	-0.64 (2.97)	-1.78 (1.96)	-1.73 (1.95)	hollow_C	1.68 (5.38)	top*
fcc	-3.21 (0.47)	-3.17 (0.44)	-3.36 (0.38)	-3.34 (0.34)	hollow_D	0.96 (4.66)	bridge*
					bridge_E	-3.22 (0.48)	-3.30 (0.28)
					bridge_F	-3.70 (0.00)	-3.58 (0.00)
NH_2					NH_2		
fcc	bridge*	bridge*	bridge*	-3.65 (0.92)	top_A	-2.88 (1.42)	-2.51 (1.53)
bridge	-3.37 (0.00)	-3.39 (0.00)	-3.64 (0.00)	-4.57 (0.00)	top_B	-3.63 (0.66)	-3.34 (0.70)
top	-3.23 (0.14)	2.83 (0.56)	-2.98 (0.66)	-1.94 (2.63)	hollow_C	-3.54 (0.75)	-3.32 (0.72)
					hollow_D	bridge*	bridge*
					bridge_E	-4.29 (0.00)	-4.04 (0.00)
					bridge_F	-3.27 (1.02)	-2.76 (1.28)

*: after structure relaxing, the NH or NH_2 diffuse to * site from the initial site.

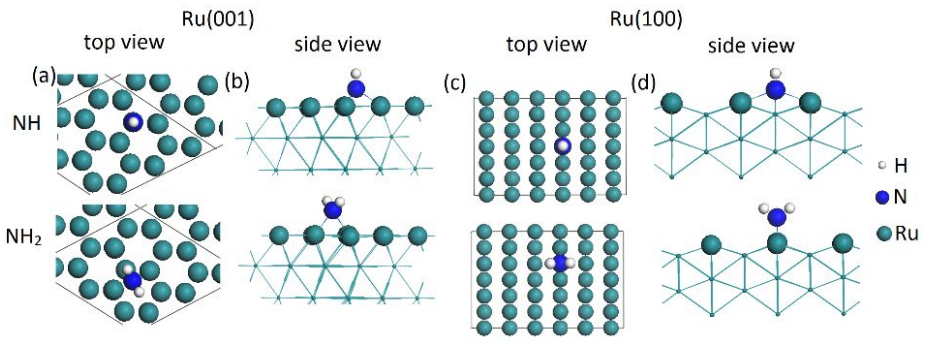

Figure 2. The configurations of the most stable adsorption of NH and NH_2 with (a) top view of Ru(001), (b) side view of Ru(001), (c) top view of Ru(100), and (d) side view of Ru(100).

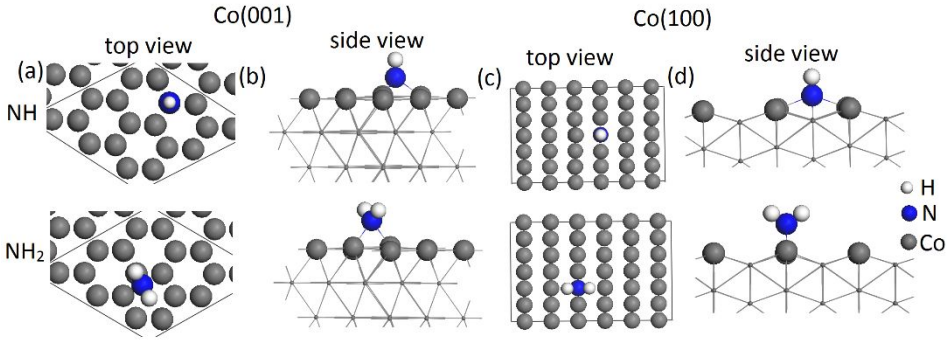

Figure 3. The configurations of the most stable adsorption of NH and NH_2 with (a) top view of Co(001), (b) side view of Co(001), (c) top view of Co(100), and (d) side view of Co(100).

on Co(001) and Co(100) surfaces and 2.01Å and 2.25Å on Ru(001) and Ru(100) surfaces. NH_2 also binds in an upright position with the nitrogen atom binding to metal atoms in bridge sites. The metal-N distances are 1.98Å and 1.95Å on Co(001) and Co(100) surfaces and 2.11Å and 2.10Å on Ru(001) and Ru(100) surfaces, respectively.

Additionally, on (001) surfaces, the metal-metal distances are 2.72Å for Ru(001) and 2.49Å for Co(001). On the (100) surfaces, the metal-metal distances between successive bridge sites are 4.29Å for Ru(100) and 4.04Å for Co(100). With this in mind, the repulsion between adsorbed NH_2 groups is stronger on the (001) surfaces. The (001) surface is flat, and NH prefers the hollow site and NH_2 prefers bridge site. However, trench structure of (100) promotes both NH and NH_2 to take different bridge sites, which are channel bridge for NH and surface bridge for NH_2. These are sufficiently well separated that the repulsion between NH_2 species is reduced on the (100) surfaces.

We have calculated the partial density of states (PDOS) of the most stable binding modes and they are shown in Figure 4 and Figure 5. We see that there is hybridization between the 2*p*-orbitals of nitrogen and *d*-orbitals of Co or Ru atom. The PDOS looks quite similar for the same adsorbate on Co or Ru surfaces. For comparison, the PDOS of the less stable binding

modes at the top site are shown in Figure S1 and Figure S2. On Ru surface, a broadened PDOS is observed at the most stable sites. On both Ru and Co surfaces, the N-2p PDOS has shifted to lower energy, resulting in stabilization at these most stable binding sites.

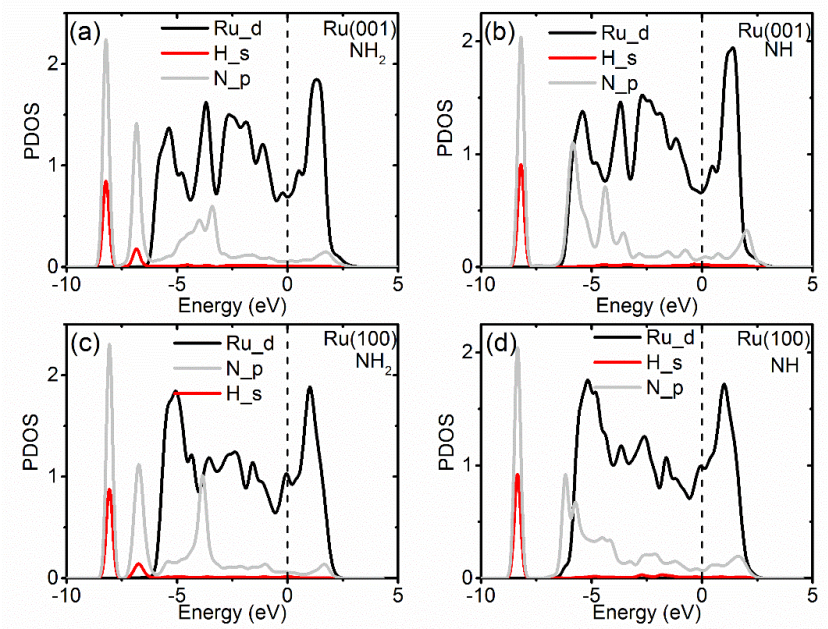

Figure 4. The plotted partial density of states (PDOS) of (a) NH_2-Ru(001), (b) NH-Ru(001), (c) NH_2-Ru(100), and (d) NH-Ru(100) at the most stable adsorption site.

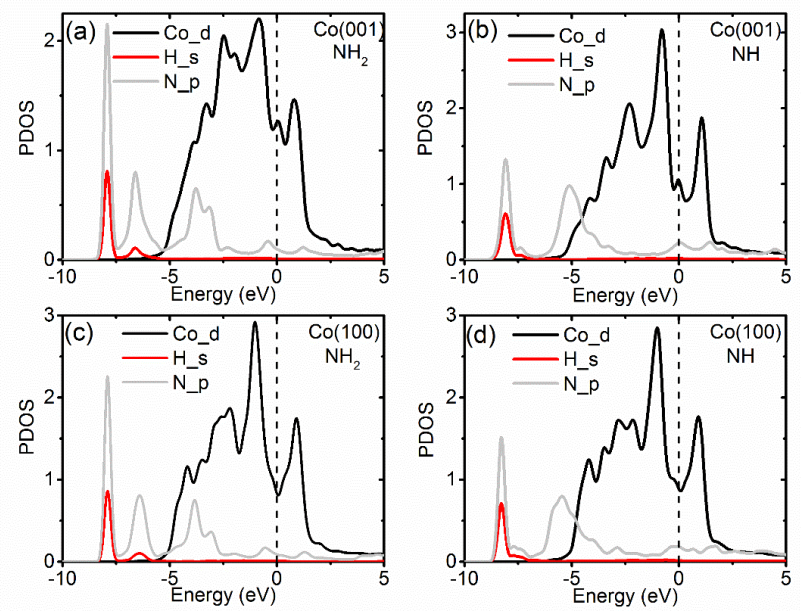

Figure 5. The plotted partial density of states (PDOS) of (a) NH_2-Co(001), (b) NH-Co(001), (c) NH_2-Co(100), and (d) Co-Ru(100) at the most stable adsorption site.

3.2 Coverage Dependence of the Stability of NH_x Terminations on Ru and Co Surfaces

Once the stable adsorption sites for single NH and NH_2 species are confirmed, we further investigate the stability of different surface coverages by increasing the number of adsorbates one by one in (3×3) unit cell. The surface coverage is defined as follows. For single adsorbate, in (3×3) unit cell, there are in total 9 possible adsorption sites. Thus, 1ML corresponds to 9 adsorbates adsorbed on the surface. In (100) surfaces, due to the zigzag structure, the adsorbate can be adsorbed on surface site and zigzag channel site. Thus, in total maximum 2ML coverage (in total 18 adsorbates) are possible with 1ML surface occupation and 1ML zigzag channel occupation.

The differential energy is defined as

$$\Delta E = E_{(n+1)A} - E_{nA} - E_A,$$

where $E_{(n+1)A}$ and E_{nA} are the energies of (n+1)*A* species on the metal surface and n*A* species on the metal surface, respectively. The reference energy for adsorbate *A* is as previously described. This differential energy is used to find the saturation coverage, where a positive differential energy means that further NH or NH_2 species cannot be accommodated on the metal surface and we are at the saturation coverage. The calculated adsorption and differential energies with respect to surface coverage are plotted in Figure 6 and Figure 7, respectively. For the adsorption energy, on (001) surfaces, these are 9 data points ranging from 1/9ML (0.11ML) to 9/9ML (1.0ML). On (100) surfaces, these are 11 data points including 9 points ranging from 1/9ML (0.11ML) to 9/9ML (1.0ML) and two points with coverages at 12/9ML (1.33ML) and 15/9ML (1.67ML). NH and NH_2 have similar adsorption strength on both (001) surfaces, while on the (100) surfaces, NH_2 clearly binds stronger than NH at all coverages. The structure of the (100) surfaces with the larger metal-metal distance and the trench appears to be able to accommodate the NH_2 species.

Considering the differential energy shown in Figure 7, on the (001) surfaces, the calculated differential energies deviate from linearity at high coverage. We have marked these deviated data points with circles in Figure 7 and carefully checked the relaxed structure. This deviation is due to the desorption of NH or NH_2 at high coverage, which leads to the formation of N_2H_2, NH_3 or NH. This allows us to then determine the most stable coverage of NH and NH_2 on all surfaces. The saturation coverage cannot be determined by differential energy alone. Although there may be negative differential energies at high coverage, the final coverage is smaller than the initial coverage. Thus, the relaxed structure at all coverages must also be considered. The configurations of all the structures at different coverages are shown in Figure S3 and Figure S4 in supporting information.

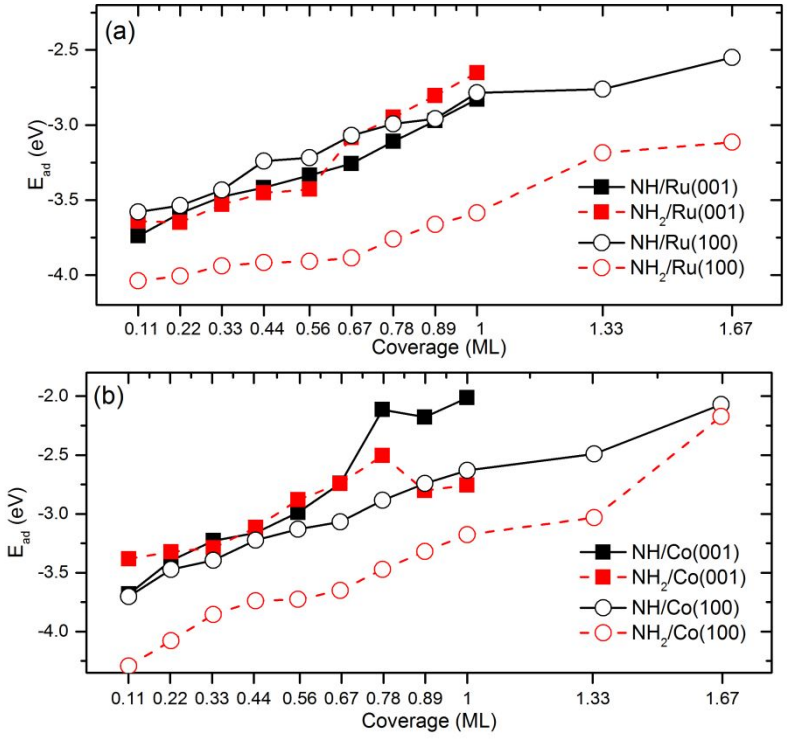

Figure 6. The calculated adsorption energies of NH and NH_2 on (a) Ru(001) and Ru(100) surfaces and (b) Co(001) and Co(100) surfaces.

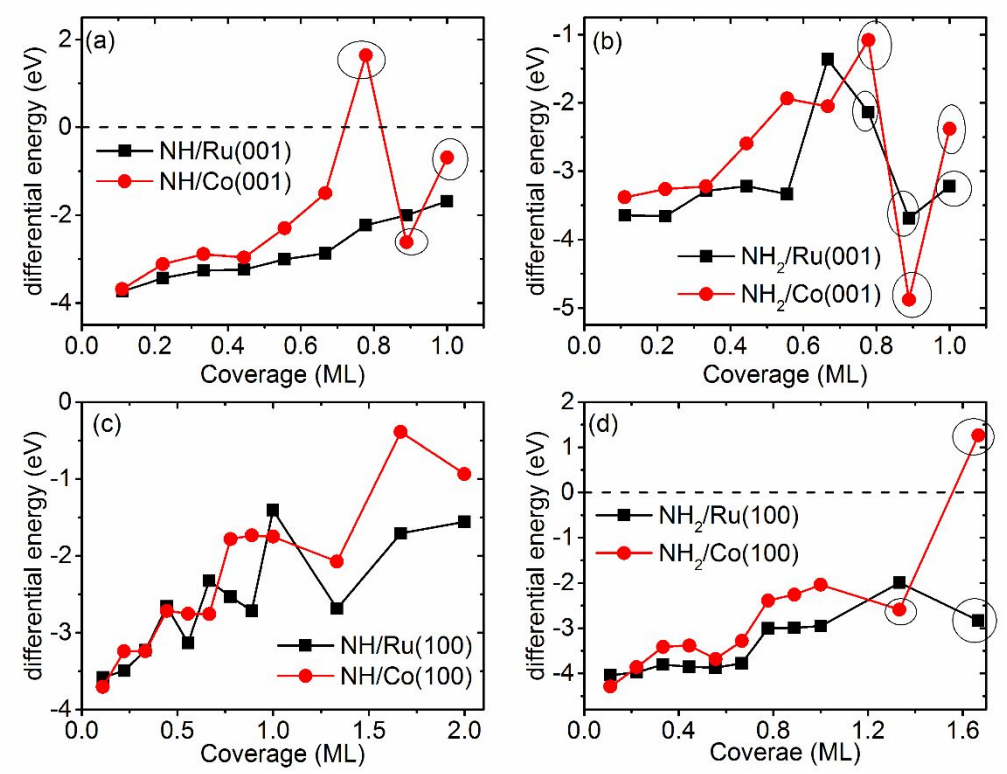

Figure 7. The calculated differential energy of NH and NH_2 on Co and Ru surfaces as a function of coverage. (a) (001)-NH terminated, (b) (001)-NH_2 terminated, (c) (100)-NH-terminated and (d) (100)-NH_2-terminated. A positive energy means that further addition of NH or NH_2 is not favourable and therefore under high coverages, NH and NH_2 would desorb from surface and NH_2 may dissociate into NH or form NH_3.

For NH species, on the Ru(001) surface, 1ML (in total 9 NH) is stable. The differential energy is negative and the relaxed structure is stable. If the number of NH is increased, the differential energy becomes positive and the extra NH species desorb from surface. Thus, the saturation coverage on Ru(001) surface of NH adsorption is 1ML. On the Co(001) surface, the differential energy becomes positive at 7/9ML (0.78ML) coverage. Although the values of the differential energy become negative again at 8/9ML (0.89ML) and 9/9ML (1.0ML), the relaxed structures of these coverages are critical to understand why the saturation coverage is no larger than 6/9ML (0.67ML). At the coverage of 0.78ML, one NH desorbs from surface and only 6 NH

are adsorbed on Co(001) surface. At the coverage of 0.89ML and 1.0ML, there is N_2H_2 formation on the surface. Thus, NH is not stable at 0.89ML and 1ML coverages. The saturation coverage on Co(001) surface of NH adsorption is 6/9ML (0.67ML). On Ru and Co (100) surfaces. Due to the unique trench structure, the differential energy is negative and the structure is stable. Thus, the saturation coverages on Ru(100) and Co(100) surfaces are 2ML.

For NH_2 species, NH_2 may dissociate into NH or form NH_3 at high coverage on (001) surfaces. On Ru(001) surface, the computed differential energies are negative for all data points. However, they are not linear at the coverage of 0.78ML, 0.89ML and 1.0ML. NH_2 is not stable on the Ru(001) surface at these coverages. For example, at 0.78ML coverage, the surface termination is 6 NH_2 and 1 NH_2 is desorbed; at 0.89ML coverage, the surface termination is 6 NH_2 and 1 NH and 1 desorbed NH_3; at 1.0 ML, the surface termination is 5 NH_2, 2 NH and 2 desorbed NH_3. Thus, the saturation coverage of NH_2 on the Ru(001) surface is 0.67ML. Similarly, on Co(001) surface, we find that NH_2 is not stable at coverages higher than 0.67ML. At 0.78ML coverage, the surface termination is 5 NH_2, 1 NH and 1 NH_3; at 0.89ML coverage, surface termination is 5 NH_2, 1 NH, 1 desorbed NH_3 and 1 desorbed NH_2; at 1ML, the surface termination is 5 NH_2, 2 NH, and 2 desorbed NH_3. Thus, the saturation coverage on Co(001) surface of NH_2 adsorption is 0.67ML.

On (100) surfaces, due to the unique trench structure, the saturation coverage of NH_2 on Ru(100) surface is 12/9ML (1.33ML). and that on Co(100) surface is 1ML. The calculated saturation coverages are summarized in Table 2. The configurations of the saturated adsorption of NH_x fragments are shown in Figure 8 and Figure 9. The structures of all the unstable high coverage NH_2 terminated surfaces are shown in Figure S3 and Figure S4 in supporting document.

The adsorbed NH_2 species can dissociate into NH and H or form NH_3 on both Co and Ru surfaces at high coverage, which shows that NH_2 is quite unstable at high coverage. The barrier for dissociation of NH_2 to NH and H on the Ru(001) surface was computed as 0.71eV in a previous DFT study.[49] Here, we have calculated the dissociation barrier for NH_2 dissociation to NH and H on the Co(001) surface using the CI-NEB method and the calculated barrier is 0.71eV, which will be easily overcome at typical ALD operating temperatures. The configurations of the initial state, transition state and final state can be found in supporting information Figure S5. This is consistent with a previous report that focused on NH_3 synthesis,[29, 49] and found that NH_2 is difficult to form but relatively easy to dehydrogenate due to high formation barrier (1.28eV) but relatively low dehydrogenation barrier (0.71eV). Additionally, as pointed out in the same report, the reaction barrier would decrease as the surface coverage increases. Our finding of NH_2 instability at high coverages supports this finding as we observe spontaneous dissociation of NH_2.

Table 2. The calculated individual saturation coverage of NH and NH_2 on Co and Ru (001) and (100) surfaces.

	Ru		Co	
	(001)	(100)	(001)	(100)
NH	1ML	2ML	6/9ML (0.67ML)	2ML
NH_2	6/9ML (0.67ML)	12/9ML (1.33ML)	6/9ML (0.67ML)	1ML

The saturation coverage of NH on Co(001) surface 6/9ML, while on Ru(001) surface full coverage of 1ML is stable. This difference between the two metals arises from the larger Ru (001) surface lattice (Ru lattice constant is 2.72Å and Co lattice constant is 2.49Å) and the

resulting larger Ru-Ru distance when compared to the Co(001) surface; Thus, the repulsion between NH groups will be weaker on the Ru (001) surface, as a result of the longer N-N distance; this distance is 2.72Å on Ru and 2.49Å on Co. The saturation coverage of NH_2 on both Ru and Co (001) surfaces is 0.67ML, so here the structural features of the metal surfaces play no role in determining the stability. At low NH_2 coverage, the interactions between adsorbed NH_2 species are not so strong. However, if the number of adsorbed NH_2 species increases, the H-H distance between two NH_2 species becomes smaller and the number of such interactions increases, the repulsion plays a more important role. This effect is more obvious on (001) surface due to smaller surface area (and smaller adsorbate-adsorbate distances) than that of (100) surface. An analysis of the relative stability at different configurations at the same coverages are summarized in Table S3 in supporting information.

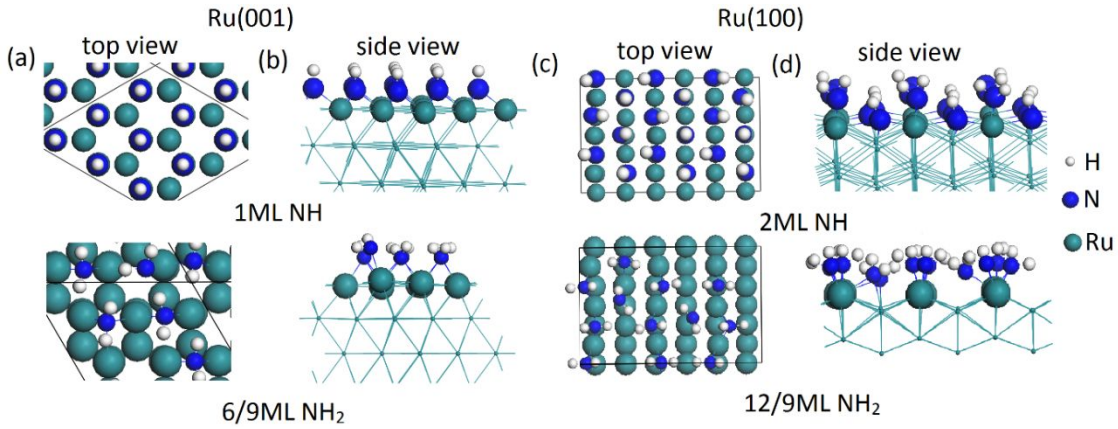

Figure 8. The configurations of the saturated adsorption of NH and NH_2 with (a) top view of Ru(001), (b) side view of Ru(001), (c) top view of Ru(100), and (d) side view of Ru(100).

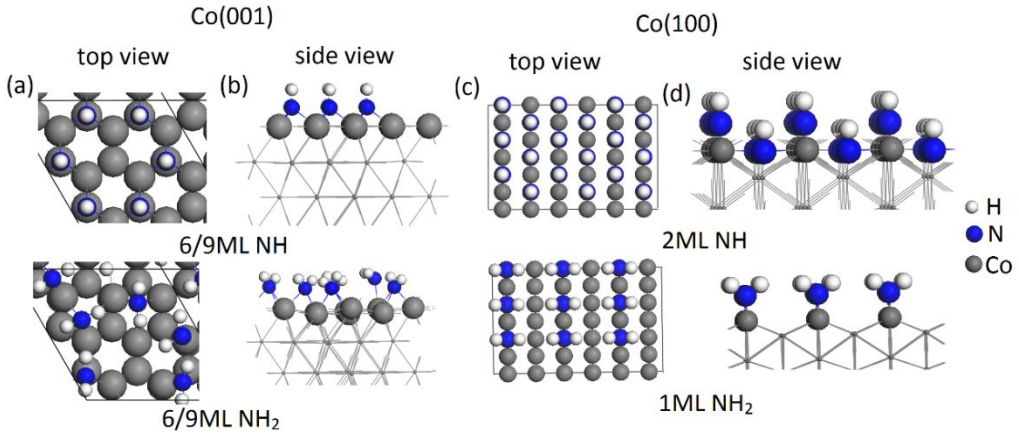

Figure 9. The configurations of the saturated adsorption of NH and NH_2 with (a) top view of Co(001), (b) side view of Co(001), (c) top view of Co(100), and (d) side view of Co(100).

3.3 Termination with Mixed NH and NH_2 Species.

We now consider the termination of the Co and Ru surfaces with a mix of NH and NH_2 species to investigate the stability of mixed NH and NH_2-terminated surfaces. On the (001) surfaces, due to the instability of adsorbed NH_2 at high coverage, an NH terminated surface model is used at the starting configuration in the simulation of mixed NH/NH_2 termination.

On the (100) surfaces, an NH_2 terminated surface model is used in the simulation of the mixed NH/NH_2 termination as a result of the greater stability of NH_2 compared to NH. All the calculations for the mixed termination cases are performed with the (3×3) surface supercell. For the Ru(001) surface, the NH saturation coverage is up to 1ML, and additional NH_2 desorbs from surface upon relaxation. Thus, Ru(001) is excluded from further discussion and will not show mixed termination with NH and NH_2.

For Co(001), the saturation coverage of NH is 6/9 ML. We start from this partial termination with NH; NH_2 species are adsorbed on available surface sites one by one until reaching full coverage. Two models with initial coverage of 5 NH and 6 NH are used. For Ru(100) and Co(100), we have considered two NH_2 terminated models: 6 NH_2 and 9 NH_2 on the (3×3) surface. Due to the stability of the NH termination, we set the number of surface NH to be 3, 6

or 9 instead of increasing the coverage of NH species one by one. These models and the energies of the mixed terminations are presented in Table 3. The configurations of models for mixed terminations are shown in Figure S6 and Figure S7 in supporting information.

Table 3. The mixed termination models and adsorption energies on Co(001) surface and (100) surfaces. The adsorption energies in the bracket are with reference to initial NH or NH_2 terminated models.

Adsorption energy/eV				
Co(001)			Ru(100)	Co(100)
$5NH+NH_2$	-2.72 (-1.35)	$6NH_2+6NH$	-3.16 (-3.24)	-2.89 (-2.72)
$5NH+2NH_2$	-2.57 (-1.51)	$6NH_2+9NH$	-2.87 (-3.00)	-2.65 (-2.67)
$5NH+3NH_2$	-2.14 (-0.73)	$9NH_2+3NH$	-3.24 (-2.20)	-2.82 (-1.76)
$6NH+1NH_2$	-2.55 (-3.88)	$9NH_2+6NH$	-3.02 (-2.17)	-2.64 (-1.83)
$6NH+2NH_2$	-2.48 (-2.95)	$9NH_2+9NH$	-2.74 (-2.70)	-2.43 (-2.23)

On all surfaces, the energy gain per adsorbate generally decreases with increasing the number of adsorbate species. On the (001) surfaces, the surface cannot reach full coverage (1ML, in total 9 adsorbates) due to the competition between NH and NH_2 and Co(001) shows a maximum of 8 adsorbates ($5NH+3NH_2$ or $6NH+2NH_2$). On the (100) surface, full coverage of mixed NH and NH_2 (2 ML, with 18 adsorbed species) is possible. This is due to the unique zigzag surface structure, which provides more available sites over a larger surface area.

3.4 Thermodynamics

NH and NH_2 prefer to bind on different adsorption sites on Co and Ru surfaces. The competition between NH and NH_2 terminations can be more deeply analysed from ab initio thermodynamics. The Gibbs free energy (ΔG) is calculated to extend the results of DFT by

adding the effect of temperature and pressure. Two values of the pressure are selected. One is the ultra-high vacuum (UHV) condition ($P/P^o = 5\times10^{-14}$) and the second is the standard ALD operating condition, taken from ref. [32] ($P/P^o = 1.97\times10^{-6}$); P^o is the standard pressure, i.e. 1 atm. For the adsorption on metal surface, the ΔG is calculated by the equation (4):

$$\Delta G = G\left[{}^{metal}/_{total}\right] - G[metal] - G_{gas}(adsorbate) \quad (4)$$

The G[metal/total], G[metal], and G_{gas}(adsorbate) are the Gibbs free energy of the metal surface (Co or Ru) with terminating groups (NH or NH_2), the clean metal, and the gas phase reference molecules (N_2 and H_2), respectively. In this study, we have ignored the changes in the vibration modes in the surface. These contributions are usually much smaller than the total energy. Therefore, we can substitute the first two Gibbs energies with DFT calculated total energies. The last term can be calculated by

$$G_{gas}(NHx) = nE_{NHx} + nG(T,P^o) + nk_BTln\left({}^{P_{NHx}}/_{P^o}\right)] \quad (5)$$

Where n is the number of adsorbate NH_x; E_{NHx} is the DFT calculated energy of the isolated NH_x species with reference to N_2 and H_2; $G(T,P^o)$ is the vibrational contribution of the NH_x species in the gas phase at different temperatures with reference to N_2 and H_2 and is calculated by VASP/Phonopy; k_B is the Boltzmann constant. Thus, for single NH or NH_2 adsorption on Ru or Co surfaces, the change in the Gibbs free energy is calculated by:

$$\Delta G(NH) = E^{(nNH)}_{NH/Metal} - E_{metal} - [n*0.5*(E_{N2} + E_{H2}) + n*0.5*\left[G^{(T,P^o)}_{N2} + G^{(T,P^o)}_{H2}\right] + nk_BTln\left({}^{P_{NH}}/_{P^o}\right) \quad (6)$$

$$\Delta G(nNH2) = E^{(nNH2)}_{NH2/Metal} - E_{metal} - \left\{n*(0.5*E_{N2} + E_{H2}) + n\left[0.5*G^{(T,P^o)}_{N2} + G^{(T,P^o)}_{H2}\right] + nk_BTln\left({}^{P_{NH}}/_{P^o}\right)\right\} \quad (7)$$

For mixed adsorption on Ru or Co surface, the change in the Gibbs free energy is calculated by:

$$\Delta G(nNH,mNH2) = E_{NH,NH2/Metal}^{(nNH,mNH2)} - E_{metal} - \left\{ n * 0.5 * (E_{N2} + E_{H2}) + m * (0.5 * E_{N2} + E_{H2}) + n * 0.5 * \left[G_{N2}^{(T,P^o)} + G_{H2}^{(T,P^o)} \right] + m\left[0.5 * G_{N2}^{(T,P^o)} + G_{H2}^{(T,P^o)} \right] + nk_B T ln\left({P_{NH}}/{P^o} \right) + mk_B T ln\left({P_{NH2}}/{P^o} \right) \right\} \quad (8)$$

Experimentally, the typical ALD deposition temperature is in the range of 350K to 650K for metal precursors.[4, 13, 38] The plotted Gibbs free energy for typical ALD operating pressure is shown in Figure 10. The plotted Gibbs free energy for ultra-high vacuum (UHV) condition can be found in Figure S8 of supporting information.

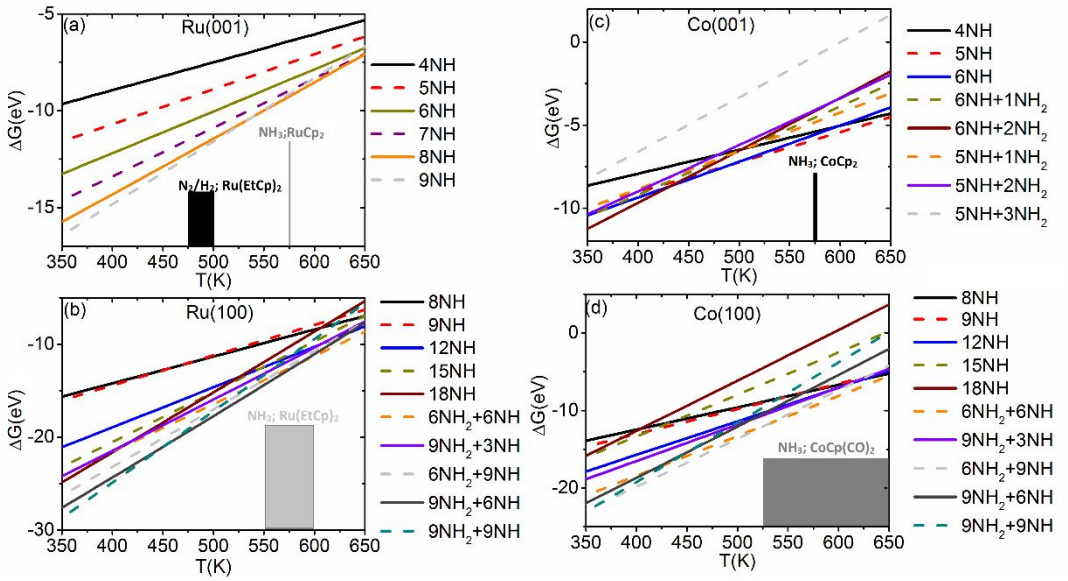

Figure 10. The plotted Gibbs free energy (ΔG) of NH_x with respect to operating temperature on (a) Ru(001), (b) Co(001), (c) Ru(100), and (d) Co(100) surfaces. The pressure is set to be ALD operating condition ($P/P^o = 1.97\times10^{-6}$). The inserts show the experimentally reported deposition temperatures taken from Ref.[4].

For Ru (001), a surface terminated with high coverage, namely 8/9ML – 1ML NH coverage is the most stable in the typical ALD operating temperature range (350K-650K). On the Co(001) surface, a surface with a partial coverage of 6/9ML NH dominates over the ALD operating temperature range between 425K and 500K and a surface with a partial coverage of 5/9ML NH dominates over the ALD operating temperature range between 500K and 650K. A Co(001) surface terminated with a mixture of NH and NH_2 (6NH and $2NH_2$) is only favorable at the lower temperature range between 350K and 425K.

Table 4. The preferred surface terminations of Ru and Co (001) and (100) surface as a functional of temperature under ALD operating condition

	Ru(3×3)	Co(3×3)
(001)	1ML NH (350K-550K); 8/9ML NH (550K-650K)	$6NH+2NH_2$ (350K-425K); 6/9ML NH (425K-500K); 5/9ML NH (500K-650K)
(100)	$9NH_2$+9NH (350K-500K); $9NH_2$+6NH (500K-600K); $6NH_2$+6NH (600K-650K)	$9NH_2$+9NH (350K-375K); $6NH_2$+9NH (375K-550K); $6NH_2$+6NH (550K-650K)

On Ru (100) and Co (100) surfaces the fully covered 9NH and $9NH_2$ surface termination is most stable at low temperature. Upon increasing the temperature, NH (or NH_2) is first desorbed from surface so that the termination changes to 6NH and $9NH_2$ (or 9NH and $6NH_2$), whereby both terminations are essentially iso-energetic. Thereafter, NH_2 (or NH) desorbs to produce a surface terminated with 6NH and $6NH_2$ on Co and Ru (100) surfaces. The results are

summarized in Table 4. Clearly, the nature of the NH_x terminated Co and Ru surfaces are temperature dependent. This can affect the adsorption strength of the metal precursors ($RuCp_2$ and $CoCp_2$) and the following Cp ligand desorption process. We can see that the growth and thin film quality of Co and Ru will therefore be sensitive to the deposition temperature and a higher deposition temperature would result in lower coverages of NH/NH_2 for Co which could impact on film quality. Thus the use of lower temperature plasma should be beneficial in promoting growth of high quality metal films.

4. Conclusions

After the plasma step in ALD, the metal surface will be NH_x terminated. Given the complete lack of knowledge of this termination, this paper focuses on the determination of the nature and stability of the NH_x terminated metal surfaces. During the subsequent metal precursor reaction, this NH_x terminated surface reacts with the metal-Cp precursor through proton transfer and ligand elimination by formation of CpH. The three most stable surfaces are (001), (101), and (100) and we choose the (001) surface, with the lowest surface energy, and the (100) surface, with high reactivity but lower stability to perform the analysis of NH_x stability. For termination with exclusively NH or NH_2, the (001) surface has a preference for NH at the hcp site while NH_2 prefers the bridge site. On the (100) surface, both NH and NH_2 prefer to bind on bridge site with channel bridge for NH and surface bridge for NH_2.

When increasing the coverage, on the (001) surface, the saturation coverage on Ru is 1ML NH and 0.67ML NH for Co. For NH_2 termination, the saturation coverages are 0.67ML on both Co and Ru surfaces. The weaker NH-NH repulsion effect on Ru surface is attributed to larger surface area compared to the corresponding Co surface. Additionally, NH_2 is unstable at high coverage by desorbing from metal surface or reacting into NH and NH_3. On the (100) surface,

the individual saturation coverage of NH on the Ru and Co surfaces are the same, namely up to 2 ML for NH. For NH_2 termination, the saturation coverages are 1.33ML on Ru and 1ML on Co surfaces.

On (001) surfaces, in a mixed termination mode, we start from the NH pre-covered surface model and add NH_2. On the (100) surfaces, an NH_2 pre-covered surface model is then modified by adding NH and NH_2. The results are analyzed with thermodynamics by calculating the Gibbs energy. Both the UHV condition and standard ALD operating condition are considered to elucidate the effect of pressure and temperature on the termination of metal surfaces. We find that under literature PE-ALD operating condition, with a temperature range of 350K-650K, and $P/P^o = 1.97\times10^{-6}$, the most stable NH_x terminated metal surfaces are 1ML NH on Ru(001) (350K-550K), 5/9 ML NH on Co(001) surface (500K-650K) and a mixture of NH and NH_2 on both Ru(100) and Co(100) surfaces. This work provides new information on the stability of NH_x terminations of metal surfaces present after nitrogen plasma step in PE-ALD and is a starting point for the further investigation of the interaction with the corresponding metal precursors. The hydrogen transfer is the key step for metal precursor interaction and the nature of NH_x termination will be expected to play an important role in the hydrogen transfer step. The effect of coverage and composition of surface terminations to the PE-ALD process is under investigation. To the best of our knowledge, there is no detailed study addressing this question yet. Experimental evidence has confirmed that the existence of N is essential in obtaining high-purity Co films.[32, 38] In the first half cycle, the precursor chemisorbed on the NH_x terminated surface and one Cp ring reacts with H atom, followed by the release of HCp. In the second half cycle, the Co ligands remaining after precursor dosing are eliminated by the NH_x radical species from the plasma. The surfaces N atom can be desorbed in the form of either NH_3 or N_2. To the best of our knowledge, the detailed study on the reaction mechanism is entirely lacking and is currently the subject of further study.

Acknowledgements

We acknowledge generous support from Science Foundation Ireland (SFI) through the SFI-NSFC Partnership program, Grant Number 17/NSFC/5279, NITRALD and the support of Prof. Zhang and Prof. Lu at Fudan. Computing resources have been generously supported by Science Foundation Ireland at Tyndall and through the SFI/HEA-funded Irish Center for High End Computing (www.ichec.ie).

Supporting Information for Publication

Calculations

Plotted densities

Configurations

References

1. Elliott, S. D.; Scarel, G.; Wiemer, C.; Fanciulli, M.; Pavia, G., Ozone-based Atomic Layer Deposition of Alumina from TMA: Growth, Morphology, and Reaction Mechanism. *Chem. Mater.* **2006,** *18*, 3764-3773.

2. Greenslit, D.; Eisenbraun, E., Characterization of Ultrathin PEALD-Grown RuCo Films for Diffusion Barrier and Copper Direct-Plate Applications. *ECS Trans.* **2011,** *35*, 17-24.

3. Chakraborty, T.; Eisenbraun, E. T., Microstructure Analysis of Plasma Enhanced Atomic Layer Deposition-grown Mixed-phase RuTaN Barrier for Seedless Copper Electrodeposition. *J. Vac. Sci. Technol. A* **2012,** *30*, 020604 1-5.

4. Miikkulainen, V.; Leskela, M.; Ritala, M.; Puurunen, R. L., Crystallinity of Inorganic Films Grown by Atomic Layer Deposition: Overview and General Trends. *J. Appl. Phys.* **2013,** *113*, 021301 1-101.

5. H., V. B.; Grillo, F.; R., V. O. J., Atomic and Molecular Layer Deposition: Off the Beaten Track. *Chem. Commun.* **2017,** *53*, 45-71.

6. Weber, M.; Julbe, A.; Ayral, A.; Miele, P.; Bechelany, M., Atomic Layer Deposition for Membranes: Basics, Challenges, and Opportunities. *Chem. Mater.* **2018,** *30*, 7368-7390.

7. George, S. M., Atomic Layer Deposition: An Overview. *Chem. Rev.* **2009,** *110*, 111-131.

8. Bilousov, O. V.; Ren, Y.; Torndahl, T.; Donzel-Gargand, O.; Ericson, T.; Platzer-Bjorkrnan, C.; Edoff, M.; Hagglund, C., Atomic Layer Deposition of Cubic and Orthorhombic Phase Tin Monosulfide. *Chem. Mater.* **2017,** *29*, 2969-2978.

9. Xie, Q.; Jiang, Y. L.; Detavernier, C.; Deduytsche, D.; Van Meirhaeghe, R. L.; Ru, G. P.; Li, B. Z.; Qu, X. P., Atomic Layer Deposition of TiO_2 from Tetrakis-dimethyl-amido Titanium or Ti Isopropoxide Precursors and H_2O. *J. Appl. Phys.* **2007,** *102*, 083521 1-6.

10. Hu, Z.; Turner, C. H., Atomic Layer Deposition of TiO_2 from TiI_4 and H_2O onto SiO_2 Surfaces: Ab Initio Calculations of the Initial Reaction Mechanisms. *J. Am. Chem. Soc.* **2007,** *129*, 3863-3878.

11. Hu, Z.; Turner, C. H., Initial Surface Reactions of TiO_2 Atomic Layer Deposition onto SiO_2 Surfaces: Density Functional Theory Calculations. *J. Phys. Chem. B* **2006,** *110*, 8337-8347.

12. Somani, S.; Mukhopadhyay, A.; Musgrave, C., Atomic Layer Deposition of Tantalum Nitride Using A Novel Precursor. *J. Phys. Chem. C* **2011,** *115*, 11507-11513.

13. Lim, B. S.; Rahtu, A.; Gordon, R. G., Atomic Layer Deposition of Transition Metals. *Nat. Mater.* **2003,** *2*, 749-54.

14. Lu, J.; Elam, J. W.; Stair, P. C., Synthesis and Stabilization of Supported Metal Catalysts by Atomic Layer Deposition. *Acc. Chem. Res.* **2013,** *46*, 1806-1815.

15. Mai, L.; Zanders, D.; Subasi, E.; Ciftyurek, E.; Hoppe, C.; Rogalla, D.; Gilbert, W.; Arcos, T. L.; Schierbaum, K.; Grundmeier, G.; Bock, C.; Devi, A., Low-Temperature Plasma-Enhanced Atomic Layer Deposition of Tin(IV) Oxide from a Functionalized Alkyl Precursor: Fabrication and Evaluation of SnO2-Based Thin-Film Transistor Devices. *ACS Appl. Mater. Interfaces* **2019,** *11*, 3169-3180.

16. Chen, Z.; Wang, H.; Wang, X.; Chen, P.; Liu, Y.; Zhao, H.; Zhao, Y.; Duan, Y., Low-temperature Remote Plasma Enhanced Atomic Layer Deposition of ZrO_2/zircone Nanolaminate Film for Efficient Encapsulation of Flexible Organic Light-emitting Diodes. *Sci. Rep.* **2017,** *7*, 40061 1-9.

17. Langereis, E.; Bouman, M.; Keijmel, J.; Heil, S.; Van de Sanden, M.; Kessels, W., Plasma-Assisted ALD of Al_2O_3 at Low Temperatures: Reaction Mechanisms and Material Properties. *ECS Trans.* **2008,** *16*, 247-255.

18. Rai, V. R.; Vandalon, V.; Agarwal, S., Surface Reaction Mechanisms During Ozone and Oxygen Plasma Assisted Atomic Layer Deposition of Aluminum Oxide. *Langmuir* **2010,** *26*, 13732-13735.

19. Leick, N.; Verkuijlen, R.; Lamagna, L.; Langereis, E.; Rushworth, S.; Roozeboom, F.; Van de Sanden, M.; Kessels, W., Atomic Layer Deposition of Ru from $CpRu(CO)_2Et$ Using O_2 Gas and O_2 Plasma. *J. Vac. Sci. Technol. A* **2011,** *29*, 021016 1-7.

20. Profijt, H. B.; Potts, S. E.; van de Sanden, M. C. M.; Kessels, W. M. M., Plasma-Assisted Atomic Layer Deposition: Basics, Opportunities, and Challenges. *J. Vac. Sci. Technol. A* **2011,** *29*, 050801 1-26.

21. Fomengia, G. N.; Nolan, M.; Elliott, S. D., First Principles Mechanistic Study of Self-limiting Oxidative Adsorption of Remote Oxygen Plasma During the Atomic Layer Deposition of Alumina. *Phys. Chem. Chem. Phys.* **2018,** *20*, 22783-22795.

22. Puurunen, R. L., Surface Chemistry of Atomic Layer Deposition: A Case Study for The Trimethylaluminum/water Process. *J. Appl. Phys.* **2005,** *97*, 121301 1-52.

23. Sun, F. Q.; Yu, J. C.; Wang, X. C., Construction of Size-Controllable Hierarchical Nanoporous TiO_2 Ring Arrays and Their Modifications. *Chem. Mater.* **2006,** *18*, 3774-3779.

24. Raymand, D.; Van Duin, A. C.; Goddard III, W. A.; Hermansson, K.; Spångberg, D., Hydroxylation Structure and Proton Transfer Reactivity at the Zinc Oxide−Water Interface. *J. Phys. Chem. C* **2011,** *115*, 8573-8579.

25. Yuzawa, H.; Aoki, M.; Otake, K.; Hattori, T.; Itoh, H.; Yoshida, H., Reaction Mechanism of Aromatic Ring Hydroxylation by Water over Platinum-Loaded Titanium Oxide Photocatalyst. *J. Phys. Chem. C* **2012,** *116*, 25376-25387.

26. Fan, C.; Chen, C.; Wang, J.; Fu, X.; Ren, Z.; Qian, G.; Wang, Z., Black Hydroxylated Titanium Dioxide Prepared via Ultrasonication with Enhanced Photocatalytic Activity. *Sci. Rep.* **2015,** *5*, 11712 1-10.

27. Novell-Leruth, G.; Valcarcel, A.; Perez-Ramirez, J.; Ricart, J. M., Ammonia Dehydrogenation over Platinum-Group Metal Surfaces. Structure, Stability, and Reactivity of Adsorbed NH_x Species. *J. Phys. Chem. C* **2007,** *111*, 860-868.

28. Novell-Leruth, G.; Valcarcel, A.; Clotet, A.; Ricart, J. M.; Perez-Ramirez, J., DFT Characterization of Adsorbed NH_x Species on Pt(100) and Pt(111) Surfaces. *J. Phys. Chem. B* **2005,** *109*, 18061-18069.

29. Logadottir, A.; Norskov, J. K., Ammonia Synthesis Over a Ru(0001) Surface Studied by Density Functional Calculations. *J. Catal.* **2003,** *220*, 273-279.

30. Popa, C.; Offermans, W. K.; van Santen, R. A.; Jansen, A. P. J., Ab Initio Density-Functional Theory Study of NH_x Dehydrogenation and Reverse Reactions on the Rh(111) Surface. *Phys. Rev. B* **2006,** *74*, 155428 1-10.

31. Kim, J. M.; Lee, H. B. R.; Lansalot, C.; Dussarrat, C.; Gatineau, J.; Kim, H., Plasma-Enhanced Atomic Layer Deposition of Cobalt Using Cyclopentadienyl Isopropyl Acetamidinato-Cobalt as a Precursor. *Jpn. J. Appl. Phys.* **2010,** *49*, 05FA10 1-5.

32. Vos, M. F. J.; G., V. S.; Kessels, W. E.; Mackus, A. J. M., Atomic Layer Deposition of Cobalt using H_2-, N_2-, and NH_3-based Plasmas: On the Role of the Co-Reactant. *J. Phys. Chem. C* **2018,** *122*, 22519-22529.

33. Lee, H. B. R.; Kim, H., High-quality Cobalt Thin Films by Plasma-Enhanced Atomic Layer Deposition. *Electrochem. Solid State Lett.* **2006,** *9*, G323-G325.

34. Kim, S. K.; Lee, S. Y.; Lee, S. W.; Hwang, G. W.; Hwang, C. S.; Lee, J. W.; Jeong, J., Atomic Layer Deposition of Ru Thin Films Using 2,4-(Dimethylpentadienyl)(ethylcyclopentadienyl)Ru by a Liquid Injection System. *J. Electrochem. Soc.* **2007,** *154*, D95-D101.

35. Klesko, J. P.; Kerrigan, M. M.; Winter, C. H., Low Temperature Thermal Atomic Layer Deposition of Cobalt Metal Films. *Chem. Mater.* **2016,** *28*, 700-703.

36. Zhu, B.; Ding, Z. J.; Wu, X. H.; Liu, W. J.; Zhang, D. W.; Ding, S. J., Plasma-Enhanced Atomic Layer Deposition of Cobalt Films Using Co(EtCp)(2) as a Metal Precursor. *Nanoscale Res. Lett.* **2019,** *14*, 76 1-7.

37. Shimizu, H.; Sakoda, K.; Momose, T.; Koshi, M.; Shimogaki, Y., Hot-wire-assisted Atomic Layer Deposition of a High Quality Cobalt Film Using Cobaltocene: Elementary Reaction Analysis on NH_x Radical Formation. *J. Vac. Sci. Technol. A* **2012,** *30*, 01A144 1-7.

38. Yoon, J.; Kim, D.; Cheon, T.; Kim, S. H.; Kim, H., Atomic Layer Deposition of Co Using N_2/H_2 Plasma as a Reactant. *J. Electrochem. Soc.* **2011,** *158*, H1179-H1182.

39. Elliott, S. D.; Dey, G.; Maimaiti, Y., Classification of Processes for the Atomic Layer Deposition of Metals Based on Mechanistic Information from Density Functional Theory Calculations. *J. Chem. Phys.* **2017,** *146*, 052822 1-11.

40. Zydor, A.; Elliott, S. D., $TiCp^*(OMe)_3$ versus $Ti(OMe)_4$ in Atomic Layer Deposition of TiO_2 with Water—Ab Initio Modelling of Atomic Layer Deposition Surface Reactions. *J. Nanosci. Nanotechnol.* **2011,** *11*, 8089-8093.

41. Shirazi, M.; Elliott, S. D., Atomistic Kinetic Monte Carlo Study of Atomic Layer Deposition Derived from Density Functional Theory. *J. Comput. Chem.* **2014,** *35*, 244-259.

42. Henkelman, G.; Uberuaga, B. P.; Jonsson, H., A Climbing Image Nudged Elastic Band Method for Finding Saddle Points and Minimum Energy Paths. *J. Chem. Phys.* **2000,** *113*, 9901-9904.

43. Phung, Q. M.; Pourtois, G.; Swerts, J.; Pierloot, K.; Delabie, A., Atomic Layer Deposition of Ruthenium on Ruthenium Surfaces: A Theoretical Study. *J. Phys. Chem. C* **2015,** *119*, 6592-6603.

44. Phung, Q. M.; Vancoillie, S.; Pourtois, G.; Swerts, J.; Pierloot, K.; Delabie, A., Atomic Layer Deposition of Ruthenium on a Titanium Nitride Surface: A Density Functional Theory Study. *J. Phys. Chem. C* **2013,** *117*, 19442-19453.

45. Kresse, G.; Joubert, D., From Ultrasoft Pseudopotentials to The Projector Augmented-wave Method. *Phys. Rev. B* **1999,** *59*, 1758-1775.

46. Perdew, J. P.; Chevary, J. A.; Vosko, S. H.; Jackson, K. A.; Pederson, M. R.; Singh, D. J.; Fiolhais, C., Atoms, Molecules, Solids, and Surfaces: Applications of The Generalized Gradient Approximation for Exchange and Correlation. *Phys. Rev. B* **1992,** *46*, 6671-6687.

47. Perdew, J. P.; Burke, K.; Ernzerhof, M., Generalized Gradient Approximation Made Simple. *Phys. Rev. Lett.* **1996,** *77*, 3865-3868.

48. Monkhorst, H. J.; Pack, J. D., Special Points for Brillouin-Zone Integrations. *Phys. Rev. B* **1976,** *13*, 5188-5192.

49. Zhang, C. J.; Lynch, M.; Hu, P., A Density Functional Theory Study of Stepwise Addition Reactions in Ammonia Synthesis on Ru(0001). *Surf. Sci.* **2002,** *496*, 221-230.

Table of Content Graphic

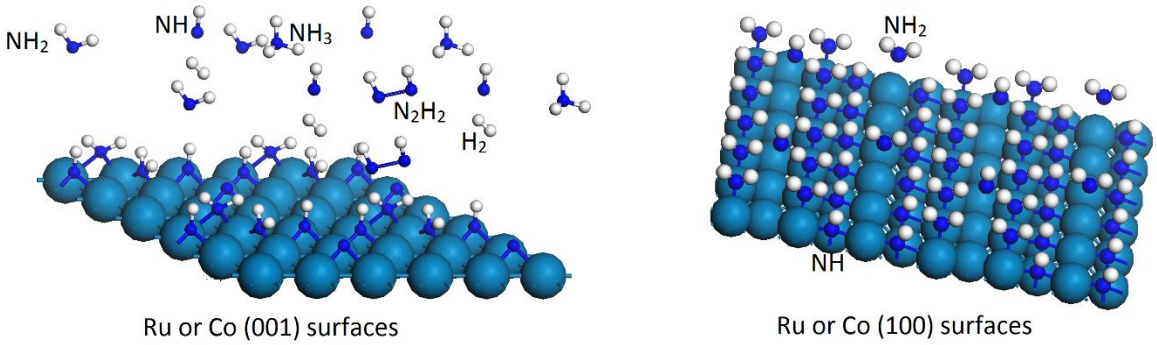

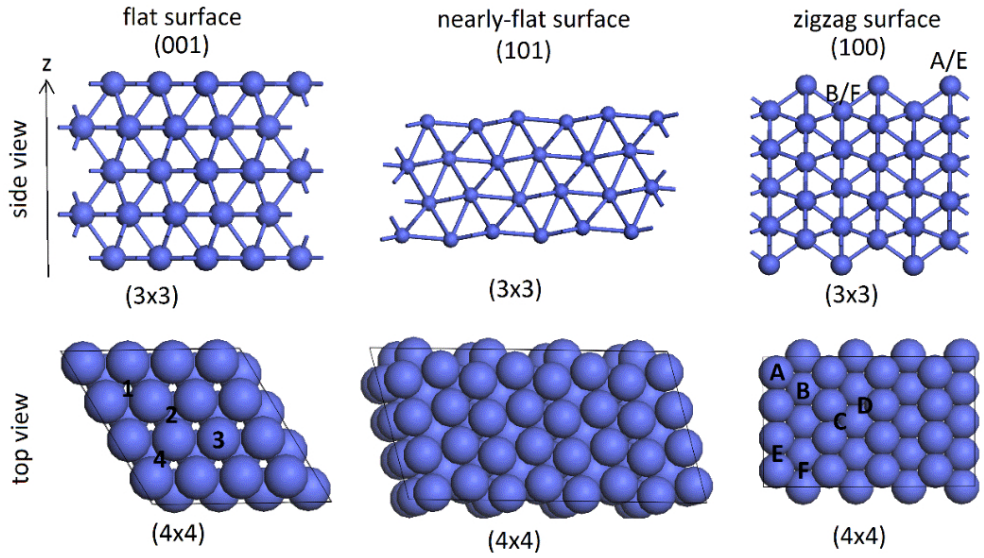

Figure 1. The top and side view of Ru or Co surfaces in three orientations: (001), (101), and (100). The adsorption sites on (001) surfaces are highlighted as 1 (fcc), 2 (hcp), 3 (top), and 4 (bridge); The adsorption sites on (100) surfaces are highlighted as A, B (top), C, D (hollow), and E, F (bridge).

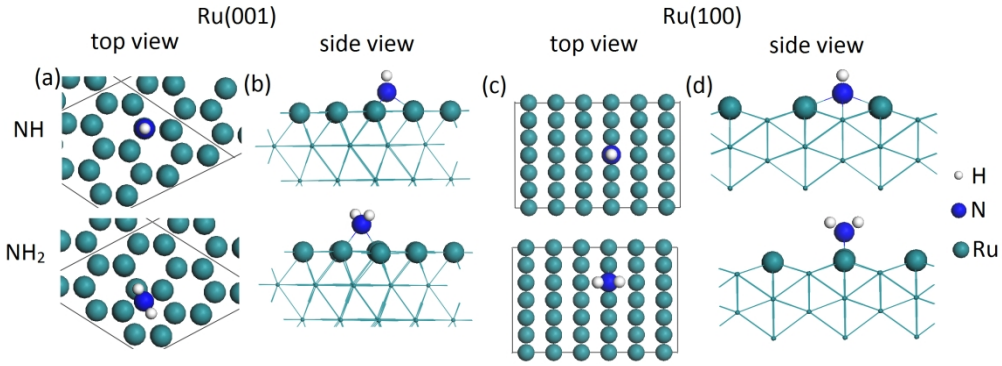

Figure 2. The configurations of the most stable adsorption of NH and NH2 with (a) top view of Ru(001), (b) side view of Ru(001), (c) top view of Ru(100), and (d) side view of Ru(100).

673x249mm (96 x 96 DPI)

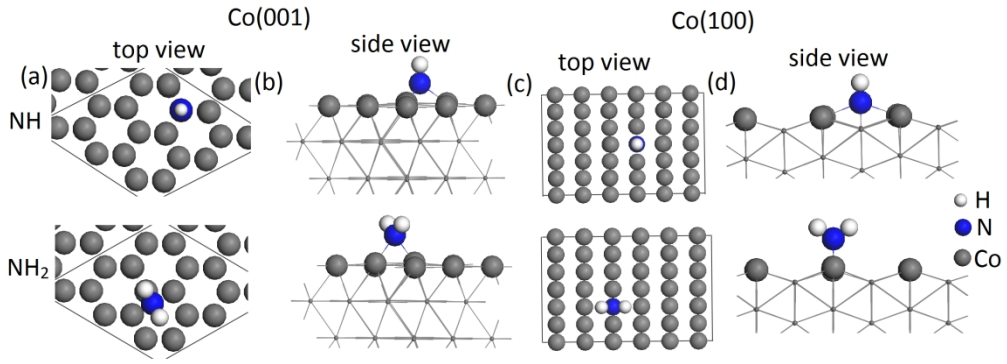

Figure 3. The configurations of the most stable adsorption of NH and NH2 with (a) top view of Co(001), (b) side view of Co(001), (c) top view of Co(100), and (d) side view of Co(100).

640x234mm (96 x 96 DPI)

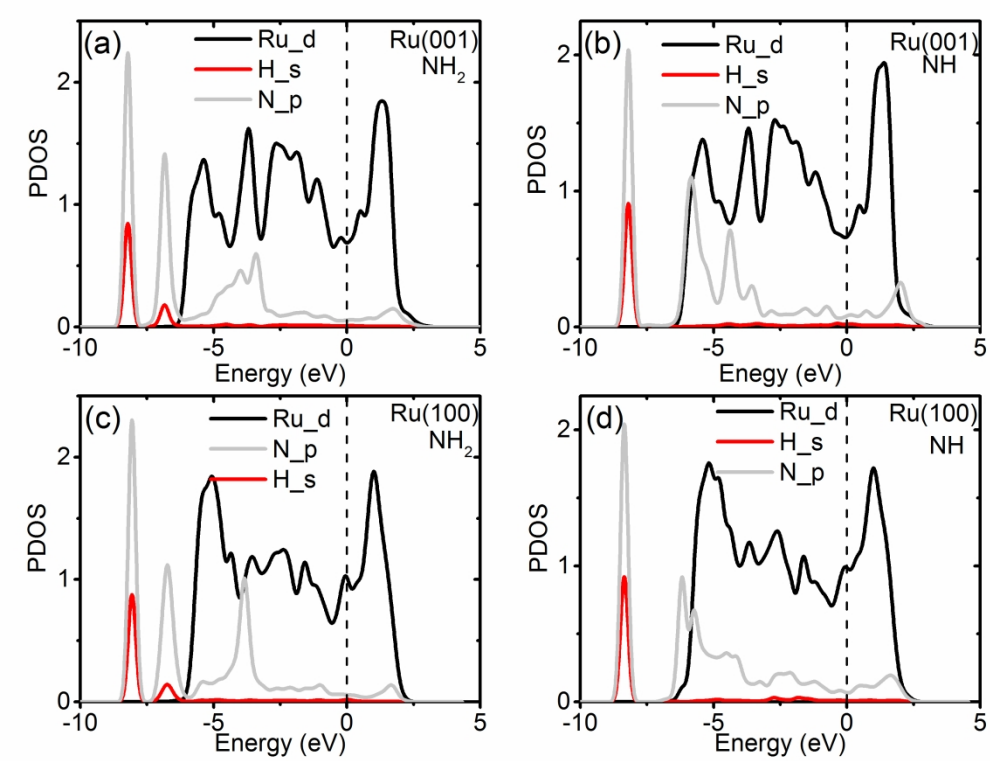

Figure 4. The plotted partial density of states (PDOS) of (a) NH2-Ru(001), (b) NH-Ru(001), (c) NH2-Ru(100), and (d) NH-Ru(100) at the most stable adsorption site.

272x208mm (300 x 300 DPI)

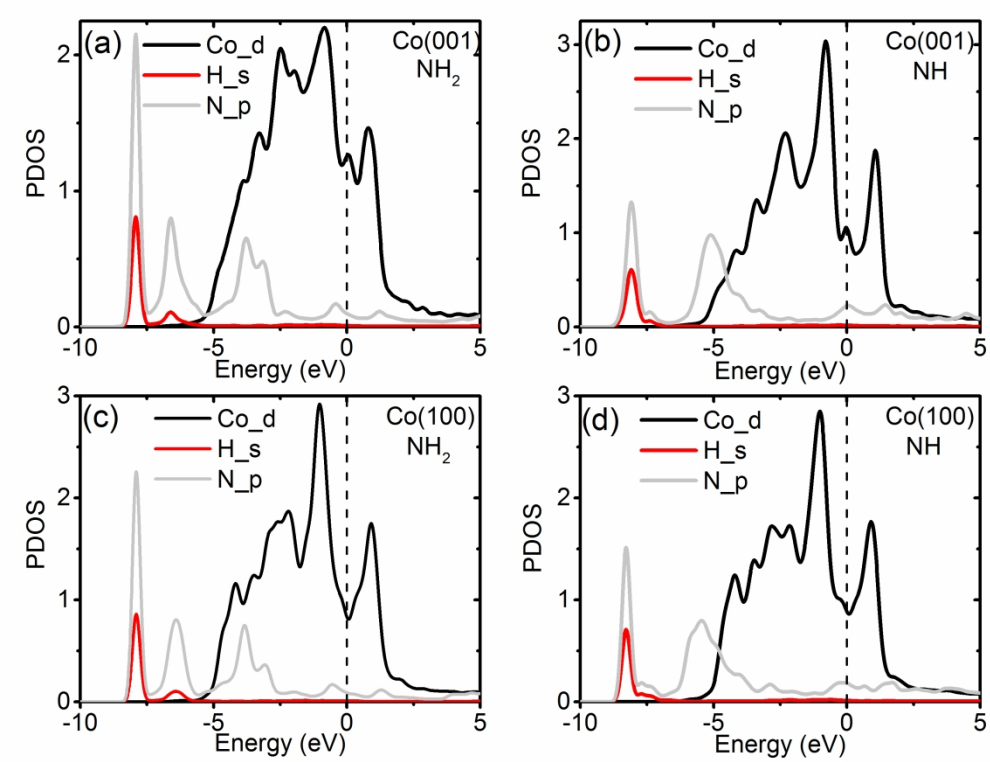

Figure 5. The plotted partial density of states (PDOS) of (a) NH2-Co(001), (b) NH-Co(001), (c) NH2-Co(100), and (d) Co-Ru(100) at the most stable adsorption site.

272x208mm (300 x 300 DPI)

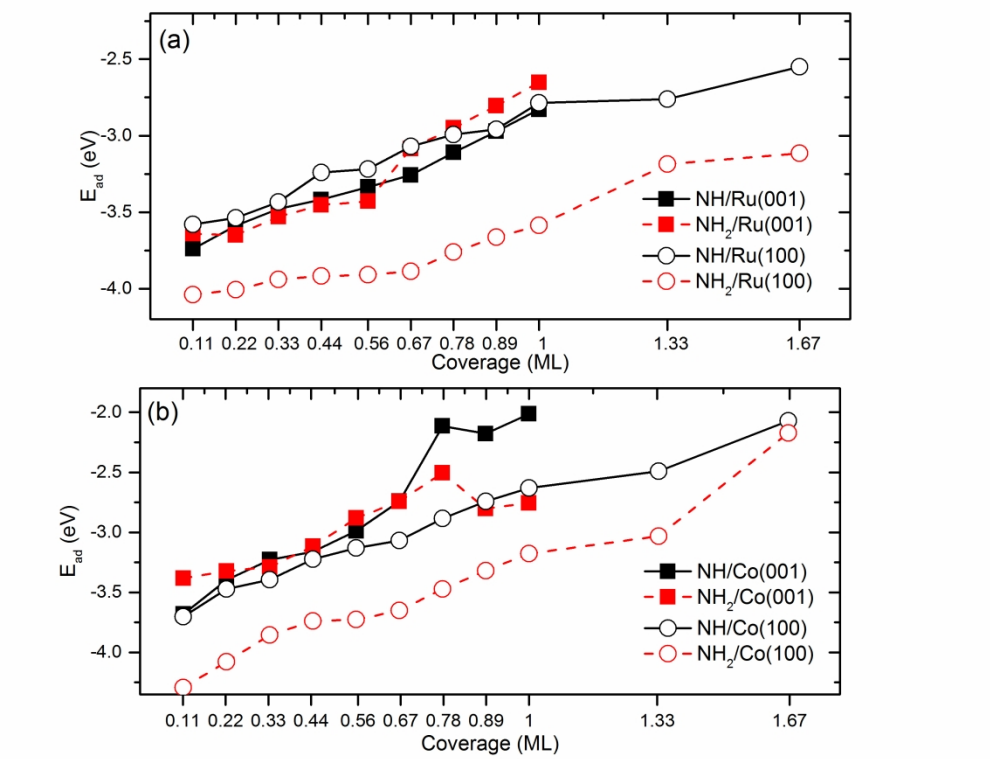

Figure 6. The calculated adsorption energies of NH and NH2 on (a) Ru(001) and Ru(100) surfaces and (b) Co(001) and Co(100) surfaces.

272x208mm (300 x 300 DPI)

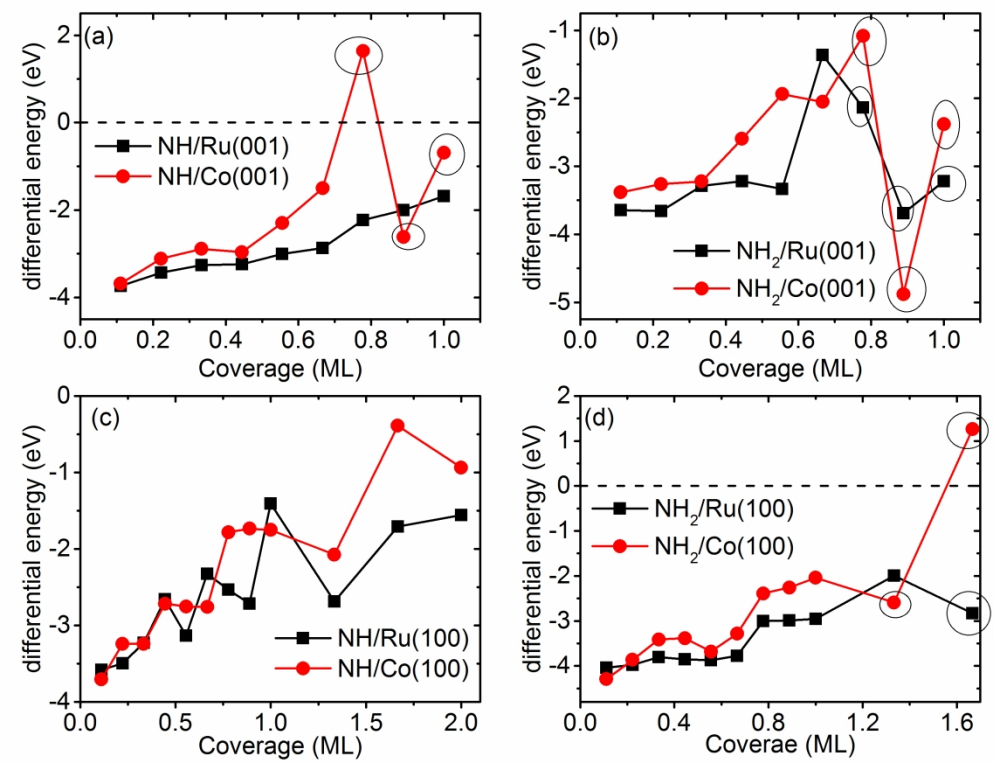

Figure 7. The calculated differential energy of NH and NH2 on Co and Ru surfaces as a function of coverage. (a) (001)-NH terminated, (b) (001)-NH2 terminated, (c) (100)-NH-terminated and (d) (100)-NH2-terminated. A positive energy means that further addition of NH or NH2 is not favourable and therefore under high coverages, NH and NH2 would desorb from surface and NH2 may dissociate into NH or form NH3.

272x208mm (300 x 300 DPI)

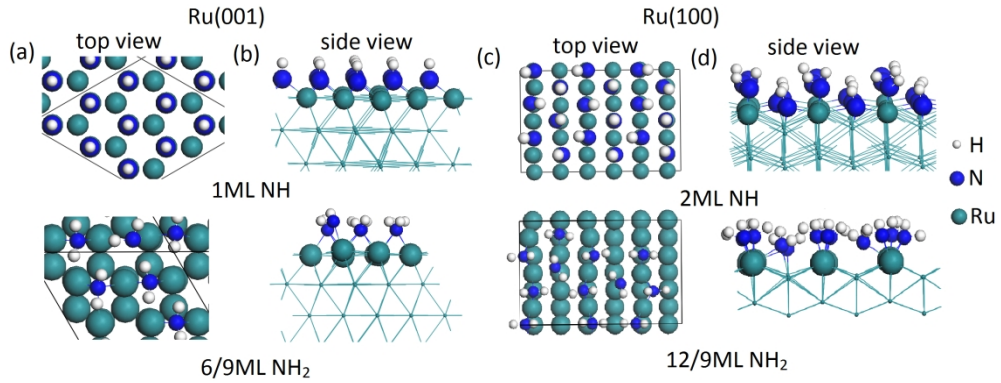

Figure 8. The configurations of the saturated adsorption of NH and NH2 with (a) top view of Ru(001), (b) side view of Ru(001), (c) top view of Ru(100), and (d) side view of Ru(100).

692x260mm (96 x 96 DPI)

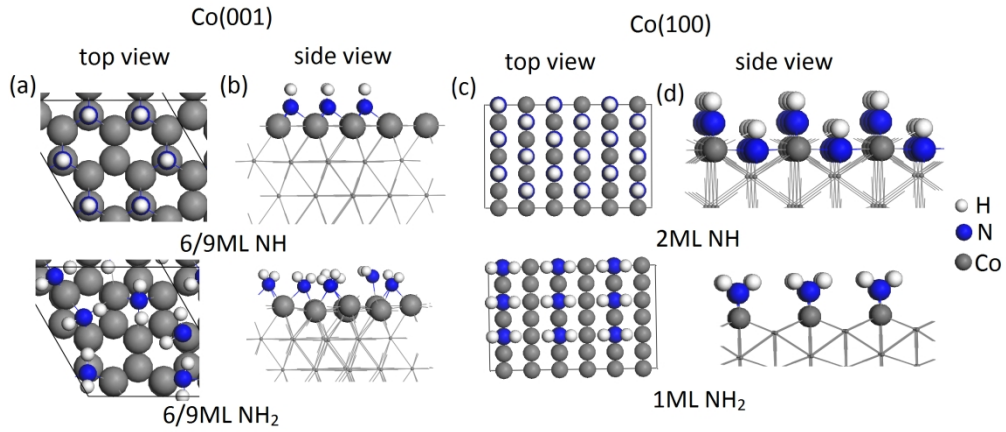

Figure 9. The configurations of the saturated adsorption of NH and NH2 with (a) top view of Co(001), (b) side view of Co(001), (c) top view of Co(100), and (d) side view of Co(100).

652x284mm (96 x 96 DPI)

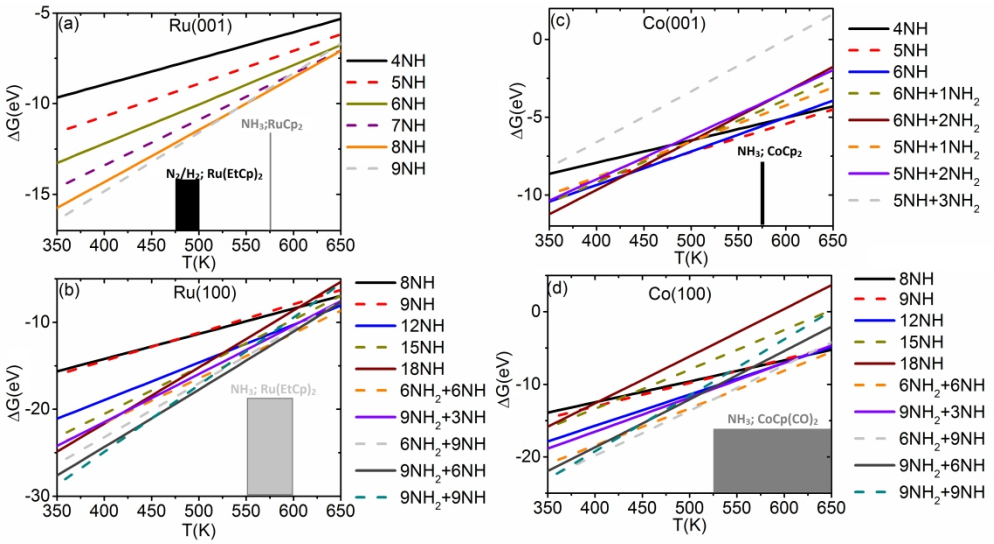

Figure 10. The plotted Gibbs free energy (ΔG) of NHx with respect to operating temperature on (a) Ru(001), (b) Co(001), (c) Ru(100), and (d) Co(100) surfaces. The pressure is set to be ALD operating condition (P/Po = 1.97×10-6). The inserts show the experimentally reported deposition temperatures taken from Ref.4.

1199x647mm (96 x 96 DPI)

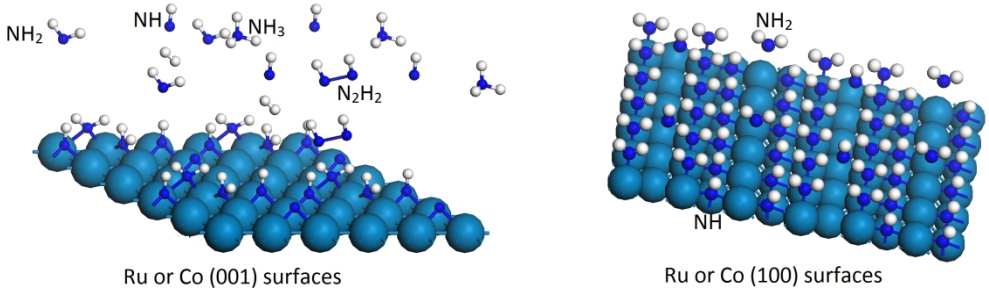

Table of Content Graphic

724x224mm (96 x 96 DPI)